

## High Speed Nanopositioning with Force Feedback

Andrew J. Fleming

**Abstract**—In this work a new method for feedback control of nanopositioning systems is proposed. A measurement of the force applied to the moving platform by the actuator is utilized as a feedback variable for both tracking and damping control. Excellent tracking and damping performance can be achieved with a simple integral controller. Other outstanding characteristics include guaranteed stability and insensitivity to changes in resonance frequency. Experimental results on a high-speed nanopositioner demonstrate an increase in closed-loop bandwidth from 210 Hz (with an integral controller) to 2.07 kHz (with force feedback control). Gain-margin is simultaneously improved from 5 dB to infinity.

### I. INTRODUCTION

Nanopositioning stages are used to generate fine mechanical displacements with resolution down to atomic scale [1]. Among other applications in nanotechnology [2], nanopositioning platforms are used widely in scanning probe microscopy [3], [4] and nanofabrication systems [5]. An example of a single degree-of-freedom lateral positioning platform is shown in Figure 1. In this device, a force developed by a piezoelectric actuator displaces the central platform to the left.

Although piezoelectric nanopositioning systems are designed to provide the greatest possible positioning accuracy, in practice, they exhibit a number of non-ideal characteristics such as creep, hysteresis and mechanical resonance that severely degrade performance [1]. As a result, all nanopositioning systems require some form of feedback or feedforward control to reduce or eliminate tracking error.

The most popular technique for control of commercial nanopositioning systems is sensor-based feedback using integral or proportional-integral control [6]. Such controllers are simple, robust to modeling error, and due to high loop-gain at low-frequencies, effectively reduce piezoelectric non-linearity. However, the bandwidth of integral tracking controllers is severely limited by the presence of highly resonant modes. It can be shown that the maximum closed-loop bandwidth is equal to the product of damping ratio  $\xi$  and natural frequency  $\omega_n$  [7], that is,

$$\text{max. closed-loop bandwidth} < 2\omega_n\xi. \quad (1)$$

This is a severe limitation as the damping ratio is usually in the order of 0.01, so the maximum closed-loop bandwidth is less than 2% of the resonance frequency. Techniques aimed at improving the closed-loop bandwidth are based on either inversion of resonant dynamics using a notch filter [8] or damped resonant dynamics using a damping controller [9], [10]. Inversion techniques are popular as they are simple to implement and can provide excellent closed-loop bandwidth, however, they also require an accurate system model and are highly sensitive to variations in resonance frequency. Damping control is more robust to changes in resonance frequency but the system is still limited by low gain margin.

This work was supported by the Australian Research Council and the Center of Excellence for Complex Dynamic Systems and Control  
 Andrew J. Fleming [andrew.fleming@newcastle.edu.au](mailto:andrew.fleming@newcastle.edu.au) is with the School of Electrical Engineering and Computer Science at the University of Newcastle, Callaghan, NSW 2308, Australia  
 Patent Pending.

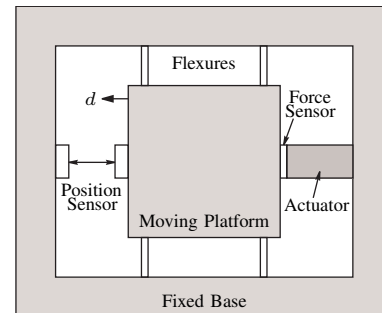


Fig. 1. A single degree-of-freedom positioning stage

The wide bandwidth of a damping controller can introduce a significant amount of sensor-induced positioning noise, which cannot be reduced in the normal way by scaling back the tracking controller gain.

In this work, a new method for feedback control of nanopositioning systems is proposed. A measurement of the force applied to the moving platform by the actuator is utilized as a feedback variable for both tracking and damping control. A major benefit of this arrangement is discussed in Section II. The system exhibits a zero-pole ordering, meaning that the resonant zeros of the system appear lower in frequency than the resonant poles. In Section III a simple integral controller is shown to provide damping performance without any limitations on gain. The system is guaranteed to be stable with a theoretically infinite gain-margin and 90 degrees phase-margin. In addition to damping control, the controller described in Section III is extended to provide tracking control without loss of performance or stability margins. As the noise generated by a piezoelectric force sensor is much lesser than a capacitive or inductive position sensor, the closed-loop positioning noise is also substantially reduced. The performance of the proposed techniques are demonstrated experimentally in Section V.

### II. MODELLING

In this section, a model is derived for the single degree-of-freedom lateral positioning platform illustrated in Figure 1. Although the model presented is simple, it adequately represents the dominant dynamics exhibited by many nanopositioning geometries.

#### A. Actuator dynamics

A typical multi-layer monolithic stack actuator is pictured in Figure 2 (a). It can be shown that a piezoelectric stack actuator can be represented as the force generator, stiffness and mass illustrated in 2 (b). The developed force  $F_a$  and stiffness  $k_a$  are [7]

$$F_a = d_{33}nk_aV_a \quad k_a = \frac{c^EA}{L}, \quad (2)$$

where  $d_{33}$  is the piezoelectric strain constant,  $n$  is the number of layers,  $V_a$  is the applied voltage,  $c^E$  is Young's elastic

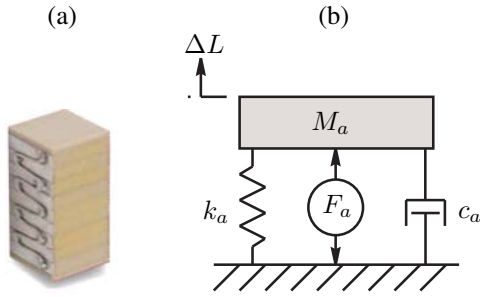


Fig. 2. (a) A Noliac monolithic stack actuator represented in (b) by a voltage dependent force  $F_a$ , stiffness  $k_a$ , effective mass  $M_a$  and damping coefficient  $c_a$

modulus under constant electric field,  $A$  is the surface area and  $L$  is the length. The ratio of developed force to applied voltage is  $d_{33}nk_a$  Newtons per Volt. In following sections, this constant will be denoted  $g_a$  where

$$F_a = g_a V_a \text{ and, } g_a = d_{33}nk_a.$$

### B. Sensor dynamics

Although the load force  $F_s$  can be measured in a number of ways, in this application it is desirable to minimize the additional mass and compliance associated with the sensor. In such scenarios, piezoelectric transducers are an excellent choice. They provide high sensitivity and bandwidth with low-noise at high frequencies. Piezoelectric force sensors can be calibrated using either voltage or charge. The open-circuit voltage  $V_s$  of a piezoelectric force sensor is

$$V_s = \frac{nd_{33}F_s}{C}, \quad (3)$$

where  $n$  is the number of layers,  $d_{33}$  is the piezoelectric strain constant,  $F_s$  is the applied force,  $C$  is the transducer capacitance  $C = n\epsilon_T A/h$  and  $A$ ,  $h$  and  $\epsilon_T$  are the area, thickness and dielectric permittivity under constant stress. The scaling factor between force and measured voltage is  $\frac{nd_{33}}{C}$  Volts per Newton. In following sections, this sensor constant will be denoted  $g_s$ , i.e.

$$V_s = g_s F_s, \text{ and } g_s = \frac{nd_{33}}{C}. \quad (4)$$

### C. Sensor Noise

Due to the high mechanical stiffness of piezoelectric force sensors, thermal or Boltzmann noise is negligible compared to the electrical noise arising from interface electronics. As piezoelectric sensors have a capacitive source impedance, the sensor noise density  $N_{V_s}(\omega)$  is due primarily to current noise  $i_n$  reacting with the capacitive source impedance, i.e.

$$N_{V_s}(\omega) = i_n \frac{1}{C\omega}, \quad (5)$$

where  $N_{V_s}$  and  $i_n$  are the power spectral densities, measured in Volts and Amps per  $\sqrt{\text{Hz}}$  respectively.

### D. Mechanical dynamics

The mechanical diagram of a single axis positioner is shown in Figure 3. The developed actuator force  $F_a$  results in a load force  $F_s$  and platform displacement  $d$ . The stiffness and damping coefficient of the flexures and actuator are denoted  $k_f$ ,  $c_f$ , and  $k_a$ ,  $c_a$  respectively.

The dynamics of the suspended platform are governed by Newton's second law,

$$M\ddot{d} + kd + c\dot{d} = F_a, \quad (6)$$

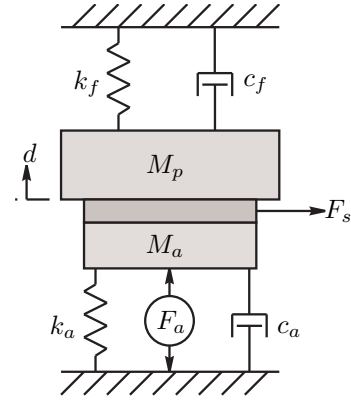


Fig. 3. Mechanical diagram of a single-degree-of-freedom positioning stage.  $F_s$  is the measured force acting between the actuator and platform mass in the vertical direction.

where  $M = M_a + M_p$ ,  $k = k_a + k_f$ , and  $c = c_a + c_f$ . The transfer function from actuator force  $F_a$  to platform displacement  $d$  is

$$\frac{d}{F_a} = \frac{1}{Ms^2 + cs + k}. \quad (7)$$

Including the actuator gain, the transfer function from applied voltage to displacement can be written

$$G_{dV_a} = \frac{d}{V_a} = \frac{g_a}{Ms^2 + cs + k} \quad (8)$$

The load force  $F_s$  is also of interest, this can be related to the actuator force  $F_a$  by applying Newton's second law to the actuator mass,

$$M_a \ddot{d} = F_a - k_a d - c_a \dot{d} - F_s. \quad (9)$$

This results in the following transfer function between the applied force  $F_a$  and measured force  $F_s$ ,

$$\frac{F_s}{F_a} = \frac{M_p s^2 + c_f s + k_f}{Ms^2 + cs + k}. \quad (10)$$

By including the actuator and sensor gains  $g_a$  and  $g_s$ , the system transfer function from the applied voltage to measured voltage can be found,

$$G_{V_s V_a} = \frac{V_s}{V_a} = g_a g_s \frac{M_p s^2 + c_f s + k_f}{Ms^2 + cs + k}. \quad (11)$$

The two system transfer functions  $G_{dV_a}$  and  $G_{V_s V_a}$ , will be used in the following sections to simulate the performance of feedback control systems. As both of these transfer functions have the same input  $V_a$  and poles, it is convenient to define a single-input two-output system  $G$  that contains both of these transfer functions,

$$G = \begin{bmatrix} G_{dV_a} \\ G_{V_s V_a} \end{bmatrix} \quad (12)$$

### E. System Properties

This transfer function  $G_{V_s V_a}$  (11) consists of a pair of resonant poles and zeros at frequencies  $\omega_z$  and  $\omega_p$ ,

$$\omega_z = \sqrt{\frac{k_f}{M_p}}, \quad \omega_p = \sqrt{\frac{k}{M}} = \sqrt{\frac{k_a + k_f}{M_a + M_p}}.$$

In general, the resonance frequency of the zeros will appear below the poles. The condition for this to occur is  $M_a k_f < k_a M_p$ . As the actuator mass  $M_a$  and flexural stiffness  $k_f$  are significantly lesser than the actuator stiffness  $k_a$  and platform mass  $M_p$ , the resonant zeros will always occur below the resonance frequency of the poles.

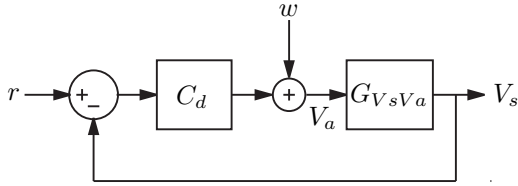


Fig. 4. A nanopositioning system  $G_{V_s V_a}$ , with input and output voltages  $V_a$  and  $V_s$  proportional to applied and measured force, controlled by an Integral Force Feedback (IFF) damping controller  $C_d(s)$

### III. DAMPING CONTROL

The technique of Integral Force Feedback (IFF) has been widely applied for augmenting the damping of flexible structures [11], [12]. The feedback law is simple to implement and under common circumstances, provides excellent damping performance with guaranteed stability [11]. In the following, IFF is applied to augment the damping of nanopositioning systems.

The feedback diagram of an IFF damping controller is shown in Figure 4.

A key observation of the system  $G_{V_s V_a}$  is that its phase response lies between 0 and 180 degrees. This is a general feature of flexible structures with inputs and outputs proportional to applied and measured force [11]. A unique property of such systems is that integral control can be directly applied to achieve damping, i.e.

$$C_d(s) = \frac{\alpha}{s} \quad (13)$$

where  $\alpha$  is the controller gain. As the integral controller has a constant phase lag of 90 degrees, the loop-gain phase lies between -90 and 90 degrees. That is, the closed-loop system has an infinite gain-margin and phase-margin of 90 degrees. Simplicity and robustness are two outstanding properties of systems with integral force feedback.

A solution for the optimal feedback gain  $\alpha^*$  has already been derived in reference [11]. This results can be adapted for the system considered in this work. Neglecting the damping, and assuming that the actuator mass  $M_a$  is negligible compared to the platform mass  $M_p$ , the optimal feedback gain  $\alpha^*$  is

$$\alpha^* = \frac{\omega_p \sqrt{\omega_p / \omega_z}}{g_s g_a} \quad (14)$$

The optimal gain can also be found numerically from the root-locus diagram of a particular system, this can be useful if the model parameters are unknown, i.e., if the system  $G_{V_s V_a}$  was procured directly from experimental data by system identification. This approach is taken in Section V.

### IV. TRACKING CONTROL

After studying the relationship between force and displacement in the following subsection, three different tracking controller architectures will be discussed.

#### A. Relationship between force and displacement

The relationship between measured force and displacement can be found by applying Newton's second law to the platform mass. The measured voltage  $V_s$  is related to displacement by

$$\frac{d}{V_s} = \frac{1/g_s}{M_p s^2 + c_f s + k_f} \quad (15)$$

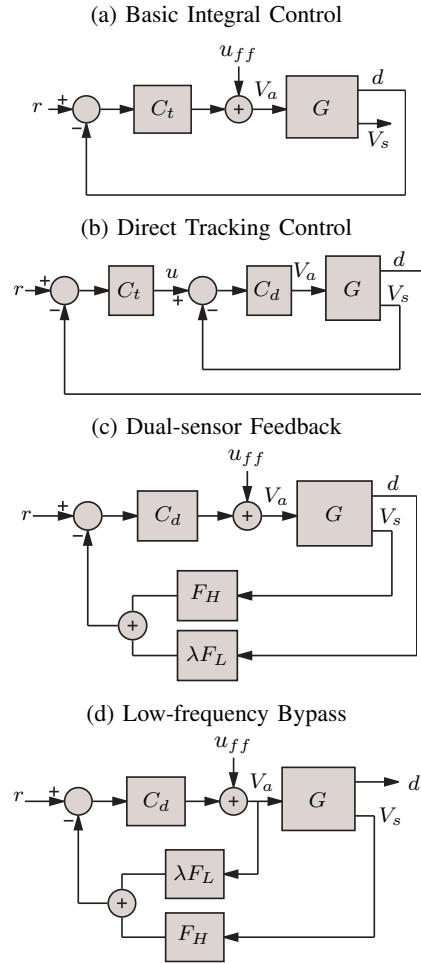


Fig. 5. The feedback diagram of a basic integral controller and three types of force-feedback controller

From this transfer function, it can be observed that displacement is proportional to force up until the frequency of the system zeros,  $\omega_z = \sqrt{k_f / M_p}$ . The scaling factor is  $g_{cl} = 1/g_s k_f$  meters per Volt. As  $V_s$  is directly proportional to displacement at frequencies below  $\omega_z$ , it makes an excellent feedback variable when trajectory tracking is required.

#### B. Integral displacement feedback

The most straight-forward technique for achieving displacement tracking is to simply enclose the system in an integral feedback loop, as pictured in Figure 5 (a). The tracking controller  $C_t$  is simply

$$C_t = \frac{\beta}{s} \quad (16)$$

In this strategy, the displacement  $d$  must be obtained with a physical displacement sensor such as a capacitive, inductive or optical sensor [13]. As discussed in the Introduction, the foremost limitation of integral tracking controllers is the bandwidth due to low gain-margin.

#### C. Direct tracking control

The low bandwidth of integral tracking controllers can be significantly improved by adding an internal force feedback loop as shown in Figure 5 (b). As the damping controller eliminates the lightly damped resonance, gain-margin is

drastically increased, allowing a proportional increase in tracking bandwidth.

To find the closed-loop transfer function, it is first convenient to find the transfer function of the internal loop. That is, the transfer function  $\widehat{G}_{du}$  from  $u$  to  $d$ , this is

$$\widehat{G}_{du} = \frac{G_d V_a C_d}{1 + C_d G_{V_s V_a}}. \quad (17)$$

The closed-loop response  $\widehat{G}_{dr}$  from  $r$  to  $d$  is then

$$\widehat{G}_{dr} = \frac{C_t \widehat{G}_{du}}{1 + C_t \widehat{G}_{du}}, \quad (18)$$

Although this scheme provides a significant bandwidth improvement, the gain-margin is still sensitive to changes in resonance frequency. In practice, the controller needs to be conservatively designed for stability with the lowest possible resonance frequency.

#### D. Dual sensor feedback

In the Section IV-A it was found that measured force is proportional to displacement at frequencies below the system zeros. A logical progression is to simply apply a reference input  $r$  to the force feedback loop and expect displacement tracking at frequencies from DC to  $\omega_z$ . Unfortunately this is not possible due to the high-pass filter formed by the piezoelectric capacitance and finite input impedance of charge amplifiers and voltage buffers.

The diagram of a dual sensor control loop is contained in Figure 5 (c). This tracking control loop is similar to Figure 4 except for the additional complementary filters  $F_H$  and  $F_L$ . These complementary filters substitute the displacement measurement  $d$  for  $V_s$  at frequencies below the crossover frequency  $\omega_c$ , which in this study is 10 Hz. The simplest choice of complementary filters are

$$F_H = \frac{s}{s + \omega_c}, \text{ and } F_L = \frac{\omega_c}{s + \omega_c}. \quad (19)$$

As the measured displacement signal  $d$  will have a different sensitivity than  $V_s$ , it must be scaled by an equalizing constant  $\lambda$ , as shown in the diagram. The value of  $\lambda$  should be

$$\lambda = \frac{G_{V_s V_a}(0)}{G_d V_a(0)} \quad (20)$$

If  $\lambda$  is chosen correctly, the closed-loop response  $\widehat{G}_{dr}$  is

$$\widehat{G}_{dr} = \frac{G_d V_a C_d}{1 + C_d G_{V_s V_a}}. \quad (21)$$

As this control loop is unconditionally stable, there is no restriction on the gain of  $C_d$ . However,  $C_d$  was chosen in the previous section to provide optimal damping performance, this value should be retained. Further increases in  $C_d$  are not productive as the disturbance rejection at the resonance frequency will degrade.

#### E. Low frequency bypass

If a physical displacement sensor is not available, or the system does not require a high level of DC accuracy, the low frequency displacement can be estimated from the input voltage  $V_a$  as shown in Figure 5 (d). This scheme can be viewed as a simple first-order observer that estimates DC position. The signal  $V_a$  requires the same sensitivity as  $V_s$  so the scaling constant is  $\lambda = G_{V_s V_a}(0)$ . If  $\lambda$  is chosen correctly, the closed-loop response and stability characteristics are the same as that discussed in the previous subsection..



Fig. 6. High-speed nanopositioning platform described in [15]

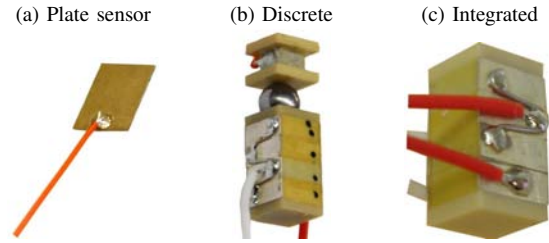


Fig. 7. Three types of piezoelectric force sensor, (a) a plate force sensor, (b) a stack actuator with discrete force sensor, and (c) a stack actuator with integrated force sensor.

#### F. Feedforward inputs

The feedforward inputs  $u_{ff}$  shown in Figure 5 can be used to improve the closed-loop response of the system [14]. Inversion based feedforward provides the best performance but the additional complexity is undesirable for the analog implementation considered in this work. A basic but effective form of feedforward compensation is to simply use the inverse DC gain of the system as a feedforward injection filter, i.e.  $u_{ff} = k_{ff} r$ . This is easily implemented and can provide a reduction in tracking lag.

#### G. Higher-order modes

So far, only a single-degree-of-freedom system has been considered. Although this is appropriate for modelling the first resonance mode, it does not capture the higher-order modes that occur in distributed mechanical systems. However, such higher order modes are not problematic as they do not disturb the zero-pole ordering of the transfer function from applied actuator voltage to the measured force.

In reference [12] it is shown that the transfer function of a generalized mechanical system with a discrete piezoelectric transducer and collocated force sensor is guaranteed to exhibit zero-pole ordering. That is, the transfer function  $G_{V_s V_a}$  will always exhibit zero-pole ordering. As the zero-pole ordering of the system is guaranteed, it follows that the controller discussed in Section III will also guarantee the stability of systems with multiple modes. The zero-pole ordering of an experimental system with multiple modes, and its successful control using the proposed technique, is reported in the following section.

## V. EXPERIMENTAL RESULTS

### A. Experimental nanopositioner

In reference [15] a high-bandwidth lateral nanopositioning platform was designed by Dr. Kam K. Leang (University of

Nevada, Reno) for video speed scanning probe microscopy. This device, pictured in Figure 6, is a serial kinematic device with two moving platforms both suspended by leaf flexures and driven directly by 10-mm stack actuators. The displacement is measured with an ADE Tech 2804 capacitive sensor.

The small stage in the center, designed for scan-rates up to 5 kHz, is sufficiently fast with a resonance frequency of 29 kHz [15]. However, the larger stage which provides motion in the adjacent axis is limited by a resonance frequency of 1.5 kHz. As this stage is required to operate with triangular trajectories up to 100 Hz, active control is required.

The main application for this nanopositioning device is high speed scanning probe microscopy. In this application, high-resolution and wide bandwidth are the most desirable characteristics. The force-feedback technique with low-frequency bypass, as discussed in Section IV-E, is the most suitable technique and will be applied here.

The platform under consideration is mechanically similar to the system in Figure 1. The major difference is the existence of higher frequency modes beyond the first resonance frequency. These can be observed in the open-loop frequency response plotted in Figure 8 (a). Although only a single mode system was previously discussed, the existence of higher order modes is not problematic. The zero-pole ordering and stability properties hold regardless of system order. This topic was discussed in detail in Section IV-G

### B. Actuators and force sensors

As discussed in Section II-B, both piezoelectric plate and stack sensors can be used to measure force. A piezoelectric plate sensor is pictured in Figure 7 (a). Also shown in Figure 7 (b) is a 10 mm Noliac SCMAP07 actuator connected to a 2 mm Nolian CMAP06 stack force sensor. The metal half-ball is used to eliminate the transmission of torsion and bending moments to the force sensor and moving platform.

For high-speed nanopositioning applications, the force sensor can also be integrated into the actuator. Such an arrangement is pictured in Figure 7 (c). The actuator is a standard 10 mm Noliac SCMAP07 stack actuator with one of the four internal actuators wired independently for use as a sensor.

Although integrated sensors are convenient and provide the highest mechanical stiffness, they also have an associated disadvantage. In addition to measuring the applied load force, an integrated sensor also detects contraction of the actuator due to Poisson Coupling as the actuator elongates. This contraction is coupled to the sensor and results in a small additive voltage opposite in polarity to the voltage induced by the load force. This error is small in systems where the flexural stiffness is appropriately matched to the stiffness of the actuator. In positioners with poorly matched actuators, i.e. where the flexural stiffness is much lesser than the actuator stiffness, the error due to Poisson Coupling can be significant. In such cases however, the error can be eliminated using the arrangement shown in Figure 7 (b).

In the following experiments, the actuator with integrated sensor is utilized. The integrated sensor simplifies the stage assembly and provides the highest mechanical stiffness.

The actuator was driven with a Piezodrive PDL200 linear amplifier. With the 250 nF load capacitance the PDL200 provides a bandwidth of approximately 30 kHz.

### C. Control design

To facilitate analysis of the control loop, a model was procured using the frequency domain subspace technique<sup>1</sup> [16]. In Figure 8 (a) the response of a 7<sup>th</sup> order, single-input, two-output identified model can be verified to closely match the system response.

The optimal control gain was determined using the root-locus technique as  $\beta=7800$ . Together with the 1-Hz corner frequency complementary filters, the controller was implemented with an analog circuit. Due to the simplicity of the control loop, analog implementation is straight-forward and has the benefits of avoiding the quantization noise, finite resolution and sampling delay associated with digital controllers.

The closed-loop frequency response is plotted in Figure 8 and reveals significant damping of the first three modes by 24, 9 and 4 dB. In addition to experimental data, the simulated response is also overlain which shows a close correlation. The tracking bandwidth of the closed-loop system is 2.07 kHz, which is higher than the open-loop resonance frequency and significantly greater than the bandwidth achievable with a direct tracking controller, predicted to be 210 Hz with a 5-dB gain-margin.

In Figure 8 (c) the linearity of the system at 100 Hz is plotted. The large ellipse in the open-loop response is due solely to hysteresis as the system phase response at 100 Hz is negligible. Due to the high loop-gain of the force feedback controller, hysteresis is effectively eliminated, even at 100 Hz.

The time domain response of the closed-loop system to an 80 Hz triangular input is plotted in Figure 8 (d). Due to the high loop-gain and resonance damping, the closed-loop response exhibits negligible induced vibration and minimal tracking lag.

## VI. CONCLUSIONS

In this work a force sensor is added to a nanopositioning stage. The resulting transfer function from applied voltage to measured force exhibits a zero-pole ordering which greatly simplifies the design and implementation of a damping controller.

In addition to damping control, the force sensor can also be used to estimate the platform displacement. This allows the damping controller to be adapted into an exceptionally high-performance tracking controller without sacrificing stability margins.

As with all piezoelectric sensors, the force sensor exhibits a high-pass characteristic at low-frequencies. This problem is solved by replacing the low-frequency force signal with a physical displacement measurement or displacement estimate based on the open-loop system dynamics.

Simulations on a nanopositioner model demonstrate the effectiveness of the proposed tracking and damping controller. The dual-sensor integral force feedback controller provides a closed-loop bandwidth approaching the open-loop resonance frequency while maintaining an infinite gain-margin and 90 degrees phase-margin. By comparison, a standard integral displacement feedback controller achieves only 5% of the bandwidth with a gain-margin of only 1 dB.

Future work involves the construction of a two-axis positioner with force-feedback for video-speed atomic force microscopy.

<sup>1</sup>A Matlab implementation of this algorithm is freely available by contacting the author.

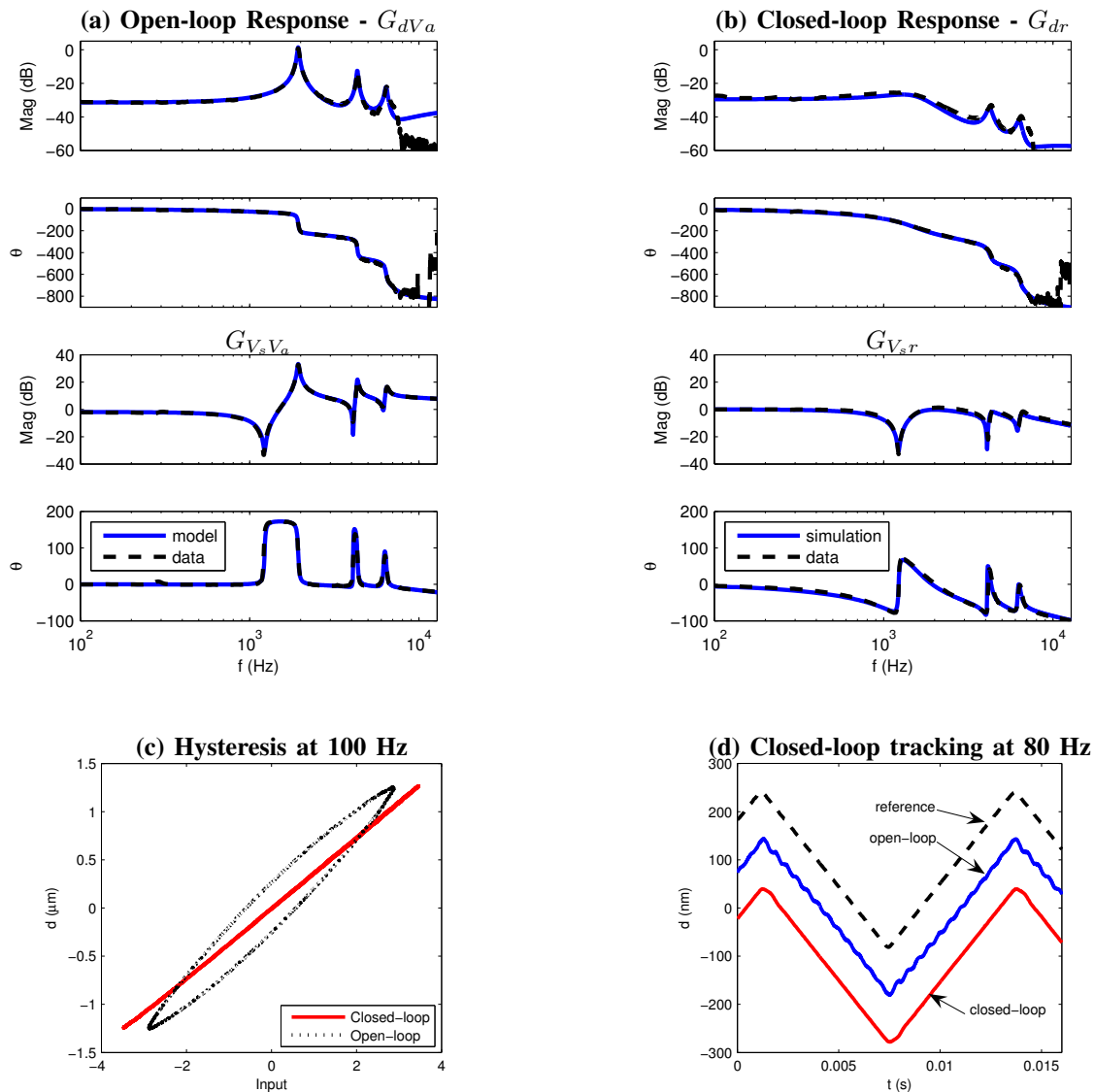


Fig. 8. The open- (a) and closed-loop (b) frequency responses of the nanopositioning system. Also plotted are the open- and closed-loop linearity (c) and response to an 80-Hz triangle wave (d). For the sake of clarity, the displacement curves in Figure (d) have been offset from each other by 100 nm.

## REFERENCES

- [1] S. Devasia, E. Eleftheriou, and S. O. R. Moheimani, "A survey of control issues in nanopositioning," *IEEE Transactions on Control Systems Technology*, vol. 15, no. 5, pp. 802–823, September 2007.
- [2] B. Bhushan, Ed., *The handbook of nanotechnology*. Springer-Verlag, 2004.
- [3] S. M. Salapaka and M. V. Salapaka, "Scanning probe microscopy," *IEEE Control Systems Magazine*, vol. 28, no. 2, pp. 65–83, April 2008.
- [4] D. Y. Abramovitch, S. B. Andersson, L. Y. Pao, and G. Schitter, "A tutorial on the mechanisms, dynamics, and control of atomic force microscopes," in *Proc. American Control Conference*, New York City, NY, July 2007, pp. 3488–3502.
- [5] A. A. Tseng, S. Jou, A. Notargiacomo, and T. P. Chen, "Recent developments in tip-based nanofabrication and its roadmap," *Journal of Nanoscience and Nanotechnology*, vol. 8, no. 5, pp. 2167–2186, May 2008.
- [6] *The world of micro- and nanopositioning (PI catalogue)*. Physique Instrumente (PI), 2005.
- [7] A. J. Fleming, "Nanopositioning system with force feedback for high-performance tracking and vibration control," *IEEE Transactions on Mechatronics*, Accepted April 2009.
- [8] D. Y. Abramovitch, S. Hoen, and R. Workman, "Semi-automatic tuning of PID gains for atomic force microscopes," in *Proc. American Control Conference*, Seattle, WA, June 2008, pp. 2684–2689.
- [9] A. J. Fleming, S. S. Aphale, and S. O. R. Moheimani, "A new method for robust damping and tracking control of scanning probe microscope positioning stages," *IEEE Transactions on Nanotechnology*, In Press, 2009.
- [10] S. S. Aphale, B. Bhikkaji, and S. O. R. Moheimani, "Minimizing scanning errors in piezoelectric stack-actuated nanopositioning platforms," *IEEE Transactions on Nanotechnology*, vol. 7, no. 1, pp. 79–90, January 2008.
- [11] A. Preumont, *Mechatronics, Dynamics of electromechanical and piezoelectric systems*. Springer, 2006.
- [12] A. Preumont, B. de Marneffe, A. Deraemaeker, and F. Bossens, "The damping of a truss structure with a piezoelectric transducer," *Computers and Structures*, vol. 86, pp. 227–239, 2007.
- [13] D. S. Nyce, *Linear position sensors. Theory and application*. John Wiley and Sons, 2004.
- [14] K. K. Leang, Q. Zou, and S. Devasia, "Feedforward control of piezoactuators in atomic force microscope systems," *Control Systems Magazine*, vol. 29, no. 1, pp. 70–82, February 2009.
- [15] K. K. Leang and A. J. Fleming, "High-speed serial-kinematic AFM scanner: design and drive considerations," *Asian Journal of Control*, vol. 11, no. 2, pp. 144–153, March 2009.
- [16] T. McKelvey, H. Akcay, and L. Ljung, "Subspace based multivariable system identification from frequency response data," *IEEE Transactions on Automatic Control*, vol. 41, no. 7, pp. 960–978, July 1996.